Journal of the European Ceramic Society 16 (1996) 773–779

0955-2219(95)00191-1
0955-2219/96/$15.00

Growth of Cubic Paraelectric Perovskite La-Modified $PbTiO_3$ Thin Films by RF Magnetron Sputtering

B. Jaber, D. Remiens & B. Thierry

Laboratoire des Matériaux Avancés Céramiques — CRITT Céramiques Fines, Université de Valenciennes et du Hainaut-Cambrésis, Z. I. Champ de l'Abbesse, 59600 Maubeuge, France

(Received 21 February 1995; revised version received 13 October 1995; accepted 24 October 1995)

Abstract

Thin films of lead titanate doped with 28% lanthanum (PLT28) have been deposited on sapphire and silicon substrates using RF magnetron sputtering. Film deposition was performed without substrate heating and the sputtering gas was pure argon. The process conditions required to prepare dense, crack-free and stoichiometric perovskite films, from different kinds of targets, have been determined. Cracking of PLT28 films on silicon substrates has been prevented by heating the substrate to 300°C during deposition. After post-annealing the films were very dense.

Les films minces de titanate de plomb dopé avec 28% en lanthane (PLT28) ont été préparés sur des substrats de saphir et de silicium par pulvérisation cathodique RF magnetron. Les dépôts sont effectués sans chauffage du substrat et le gaz de pulvérisation est de l'argon pur. Les conditions de process nécessaires pour préparer des films PLT28 stoechiométriques, de structure pérovskite, denses et sans fissures ont été determinées. Les fissures apparaissant sur les films déposés sur silicium ont été supprimées par chauffage du substrat à 300°C durant la croissance du film. Après le traitement thermique les films sont très denses.

1 Introduction

Ferroelectric ceramics belonging to the solid solution system PLZT (lead–lanthanum zirconate–titanate) have undergone substantial technology development due to their many interesting properties. These materials can be piezoelectric, ferroelectric, electrooptic, pyroelectric, ... but in the bulk form, the use of these ceramics has been limited by the relatively high switching voltages required.

Many techniques[1–4] have been developed to grow these materials in thin films form. Such films allow the inherent limitations of monolithic ceramics to be overcome and to attain compatibility with semiconductor technologies.

Among these methods, cathodic sputtering, DC or RF, is the most developed[5,6] to prepare ferroelectric thin films such as lead titanate (PT), lead zirconate–titanate (PZT) and PLZT. There have been numerous proposals for the application of the PLZT thin films in optoelectronic devices, in particular the (28/0/100) composition which exhibits interesting electrooptic effects superior to those of $LiNbO_3$ as shown in Table 1.

The purpose of this paper is to report the preparation of PLT28 thin films on sapphire and silicon substrates. Deposition conditions and post-annealing parameters have been optimised in order to produce stoichiometric thin films with perovskite structure.

2 Experimental Procedure

The radio-frequency magnetron sputtering system used was described previously.[9] For easy target fixation, the deposition has been performed in the 'sputter-down' mode. The substrate temperature was measured by a chromel-alumel-type thermocouple placed just behind the substrate. The measured temperature, as reported in this paper, represents the substrate block temperature. Films are deposited on substrates of (0001) sapphire and (100) oxidised silicon. The properties of the substrates

Table 1. Comparison of the linear electrooptic coefficient r for some materials

Material	r 10^{-10} *(m/V)*	*Ref.*
PLZT (9/65/35)	0·22	7
PLZT (28/0/100)	0·35-0·41	7
$LiNbO_3$	0·17	8

Table 2. Characterisation of the substrates used and of PLT28 ceramics

Material	*Structure*	*(hkl)*	*Lattice parameter (Å)*	*Thermal expansion coefficient* $10^{-6}K^{-1}$	*Ref.*
Al_2O_3	Rhombohedral (α-Al_2O_3)	(0001)	a = 4·759 c = 12·991	7·5	10
Si	Diamond cubic	(100)	a = 5·4301	3	10
PLT28	Perovskite cubic	—	a = 3·9277[11]	6·6 $623 \leq T \leq 773$ K	12

used and of PLT28 ceramics are summarised in Table 2.

Before deposition, all substrates were cleaned in a series of organic solvents and deionised water.

Different types of targets were studied:

— A mixture of PbO, TiO_2 and La_2O_3 powders (purity >99·95%) with the composition of $Pb_{1-x}La_xTi_{1-x/4}O_3$ where x = 0·28. The target diameter and thickness were 3" and 3 mm, respectively. This chemical formula has been used assuming the B-site vacancies to neutralise the extra-positive charge from the La addition–creation (La^{3+} occupies the A-sites (Pb^{2+}) in the tetragonal perovskite structure of $PbTiO_3$). Films made using this formula had better optical and electrical properties.[13]

— Reacted powder prepared by calcination of a mixture of oxides for 6 h at 1100°C. The stoichiometry of this powder was confirmed by Inductively Coupled Plasma (ICP) analysis. X-ray diffraction showed the powder to have the cubic perovskite structure with lattice parameter of a = 3 9303 Å.

— Sintered target prepared by pressureless sintering of the reacted powder at 1250°C for 4 h, using a powder bed of $PbZrO_3$ (to prevent the lead evaporation). The latter two targets had a 1" diameter and 2 mm thickness.

In order to stabilise the target surface composition (formation of the 'altered layer') and to remove the adsorbed gas, a pre-sputtering run was necessary:

— 3 h for the new target.

— 30 min before each deposition for a previously used target.

The pre-sputtering conditions were identical to those of deposition.

After carrying out many depositions, cracks appeared in the erosion track of all targets probably due to local heating provoked by the presence of the magnetron system.

3 Film Characterisation

The thickness and its uniformity of the PLT28 films were measured by profilometry with 200 Å precision. The film was then chemically etched (hydrochloric acid) to make a step between the film and the substrate (obtained by photolithography). The film composition was analysed by ICP. The structure was determined by X-ray diffraction (XRD) with a counter diffractometer using θ–2θ geometry and Cu Kα radiation. The film morphology was examined by scanning electron microscopy (SEM).

4 Results and Discussion

It is well known that the deposition conditions such as RF power density, gas pressure, target–substrate distance, ..., affect the properties of films, primarily the deposition rate, the film composition as well as the microstructure.

4.1 Deposition rate

The effect of argon pressure on different types of target (1" diameter) have been studied. Figure 1 shows the deposition rate variations versus the

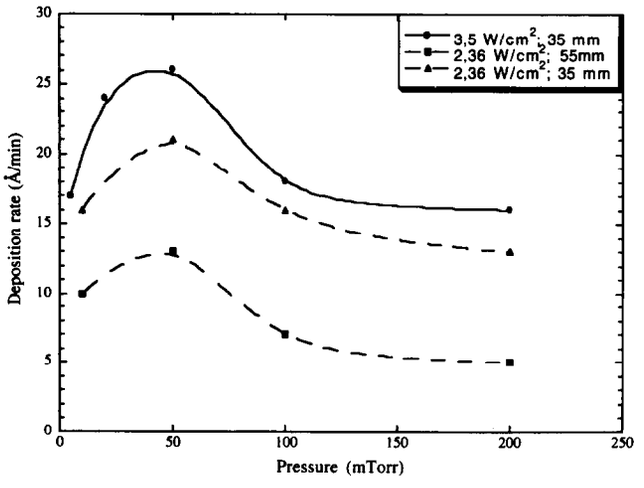

Fig. 1. Deposition rate variations versus argon pressure for two values of power density: 2·36 and 3·5 W/cm^2 and two inter-electrode distances: 35 and 55 mm. A mixed oxide powder target (1" diameter) and a silicon substrate were used.

argon pressure for two values of power density: 2·36 and 3·5 W/cm^2 and two inter-electrode distances: 35 and 55 mm, in the case of the mixed oxide powders target. The deposition rate was deduced by the film thickness measurement divided by the duration of sputtering.

Below 50 mTorr, the deposition rate increased with the argon pressure, since the ion density increased. The deposition rate decreased when the pressure become larger than 50 mTorr; the number of collisions in the reactor increased therefore the ion efficiency decreased. Above 100 mTorr, the deposition rate was constant; in the order of 15 Å/min for an RF power density of 2·36 W/cm^2 and an inter-electrode distance of 35 mm. It was likely that the backscattering effect contributed to these effects at high pressure.

The increase of RF power density involved an increase of the deposition rate since the Ar^+ energies increased which causes an increase in the density of sputtered neutrals and their average energy. However, the deposition rate decreased when the distance between the target and substrate increased, in effect, the energy of the Ar^+ decreased as the number of collisions increased and in addition the sputtered neutrals were thermalised near the target which increased the diffusion path.

As can be seen in Fig. 2, the deposition rate also depended on the type of target. For fixed deposition conditions the highest film deposition rate was obtained using the sintered target. These variations were presumably due to the large differences in the kinds of sputtered neutrals and in the bonding energies of species at the surface of each target types.

Sintered targets which often broke after each deposition were rejected. This behavior was probably due to the large stress generated in the material because of the large quantity of dopant (28% lanthanum) incorporated.

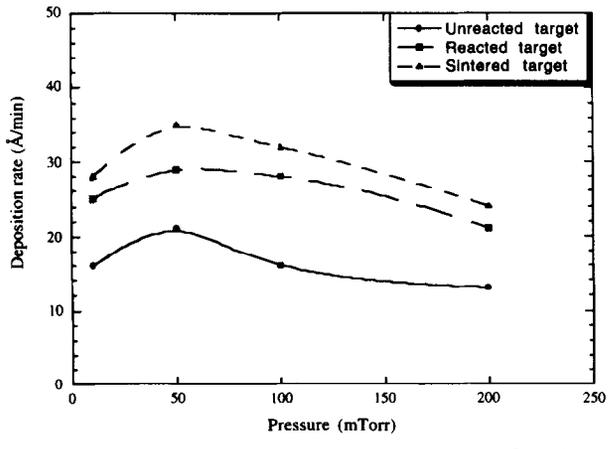

Fig. 2. Deposition rate versus gas pressure as a function of target type, RF power density density P_{rf} = 2·36 W/cm^2, sputtering pressure P = 100 mTorr, target–substrate distance d = 35 mm.

4.2 Film composition

In this study two types of targets were used.

4.2.1 Target of reacted powder (1" diameter)

As previously mentioned, film deposition was carried out at room temperature. The substrate temperature reaches about 50°C during the deposition phase due to electron/ion bombardment. Figure 3 shows the film composition variations versus the RF power density; the sputtering pressure and the inter-electrode distance were fixed at 50 mTorr and 35 mm respectively. Whatever the RF power density the concentrations of Pb and Ti were far from the desired composition. However the desired concentration of La is obtained for RF power density of 1·2 W/cm^2. Therefore this RF power density was selected to study the pressure effect on the film composition. As can be seen in Fig. 4, a working point for this type of target was found for an Ar pressure about 110 mTorr. Contrary to that found previously for $PbTiO_3$ films,[9] PLT28 films investigated in this study did not contain an excess of Pb. These is presumably due to the large quantity of La^{3+} (28%) occupying the Pb^{2+}-site in the $PbTiO_3$ perovskite and to the

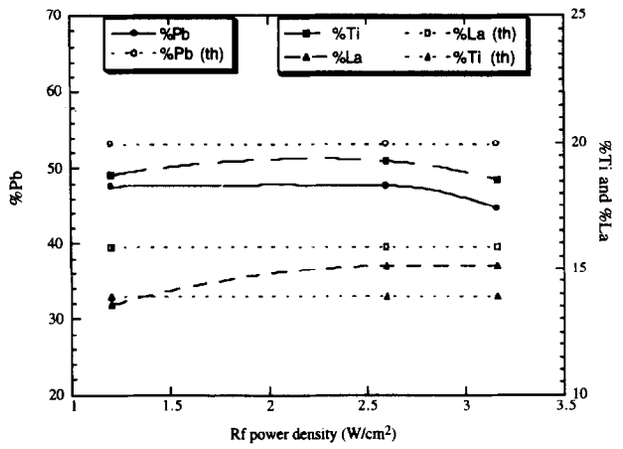

Fig. 3. Film composition versus RF power density for Al_2O_3 substrate with the reacted powder target (1" diameter); P = 100 mTorr and d = 35 mm.

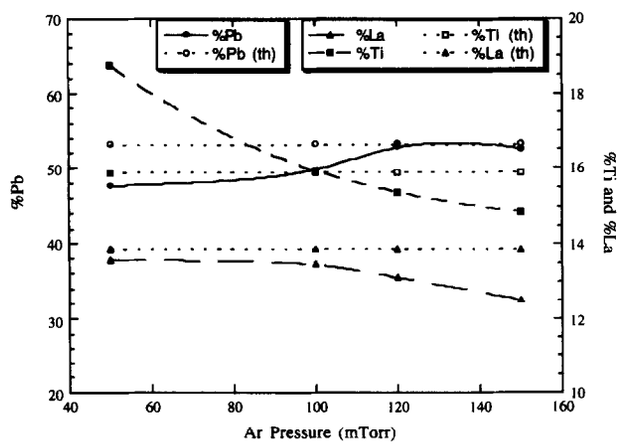

Fig. 4. Film composition versus argon pressure for Al_2O_3 substrate with the reacted powder target (1" diameter); P_{rf} = 1·2 W/cm^2 and d = 35 mm.

difference in the transfer process of the sputtered species.

4.2.2 Target of mixed oxide powders (3" diameter)
The object with this type of target was to attain an excellent uniformity of film thickness and composition.

In this context, the distance between target and substrate was fixed at 70 mm for 50 mTorr pressure (the thermalisation regime was certainly attained). Figure 5 illustrates the composition variation versus the RF power density for a fixed argon pressure of 50 mTorr. Elemental concentration varied very little with the RF power density.

The composition variations versus the sputtering pressure (RF power density fixed at 2·6 W/cm^2) are shown in Fig. 6. The observed behavior was different to that obtained in the case of the reacted powder target particularly for Ti and La elements.

From these studies, optimised deposition conditions were defined and are summarised in Table 3.

For these sputtering conditions and with these target diameters the substrate temperature reaches about 170°C during deposition due to the ion bombardment. Using this target and the optimal

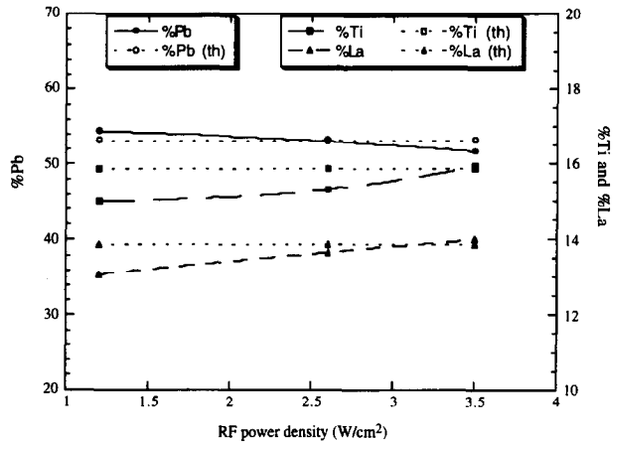

Fig. 5. Variation of the film composition as a function of the RF power density for Al_2O_3 substrate with the unreacted powder target (3" diameter); P = 50 mTorr and d = 70 mm.

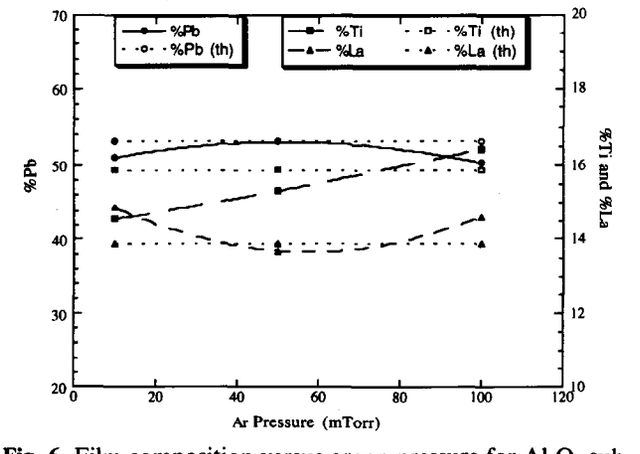

Fig. 6. Film composition versus argon pressure for Al_2O_3 substrate with the unreacted powder target (3" diameter); P_{rf} = 2·6 W/cm^2 and d = 70 mm.

Table 3. Optimal deposition parameters of unreacted powder target

Inter-electrode distance	70 mm
RF power density	2·6 W/cm^2
Sputtering gas	100% Ar
Gas pressure	50 mTorr
Substrate temperature	~170°C

conditions, the effect on the film composition of the oxygen concentration in the sputtering gas (argon) has been investigated. As can be observed in Fig. 7, the incorporation of 5% O_2 in Ar resulted in a decrease of different element concentrations. Above this quantity of O_2 the composition remained constant. These observed variations are likely to arise from the high reactivity of O_2 with these elements at the target surface as well as in the plasma.[14]

4.2.3 Composition reproductibility
In Fig. 8 the results obtained for films made under the optimised conditions (Table 3) from 3" targets (mixed oxide powders) are presented. Composition reproducibility of 4% was found for films produced from the same target (data points 1 and 2) as well as for films obtained from different targets

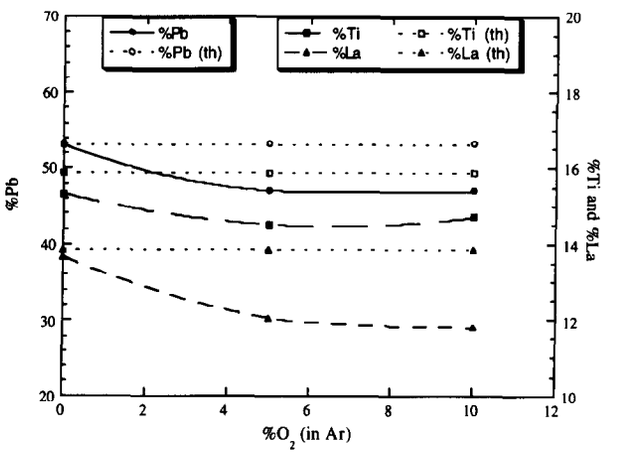

Fig. 7. Effect of oxygen concentration in the sputtering gas (Ar) on the film composition.

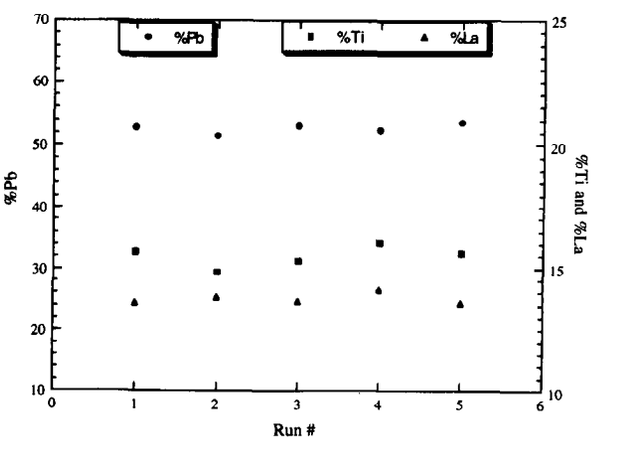

Fig. 8. Film composition reproducibility for the unreacted powder target (3" diameter).

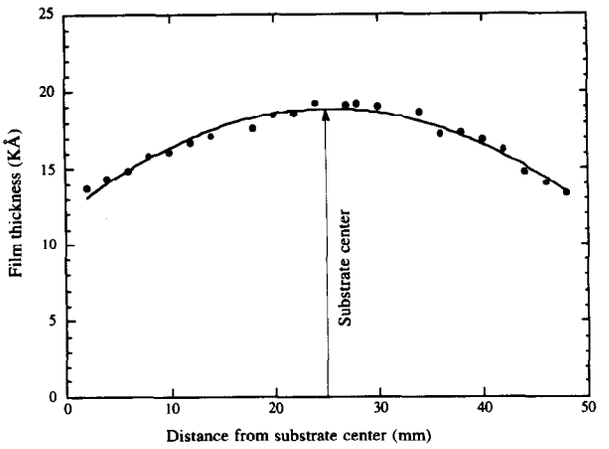

Fig. 9. Variation of the film thickness as a function of the radial distance from the substrate centre.

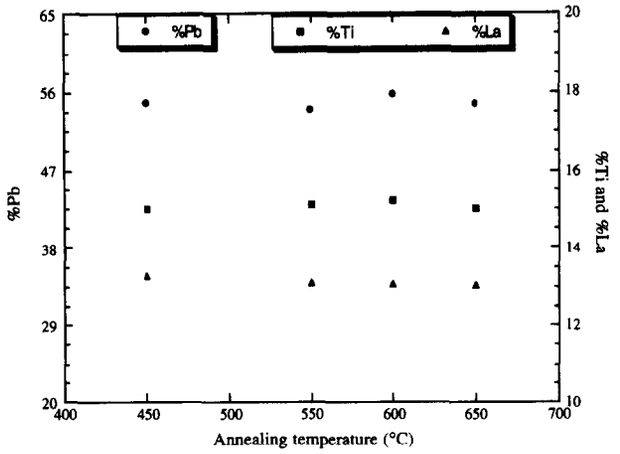

Fig. 11 Film composition as a function of the annealing temperature. Annealing time = 2 h.

(data points 3, 4 and 5). These composition deviations were attributed to the analysis error of the ICP.

4.2.4 Thickness uniformity

Films were deposited on silicon substrates 2" in diameter from 3" diameter targets of unreacted powder. The desired film thickness was about 1·9 μm (for our future applications). Figure 9 shows film thickness as a function of the radial distance from the substrate centre.

The observed variation was due to the inner and outer diameters of the plasma ring (magnetron effects) and to the variations in the ejection angles for the sputtered species.[15] For the present deposition conditions the inner and the outer diameters of the plasma ring (Fig. 10) are estimated to be 1·7 and 2·7 mm respectively. A 5% film thickness uniformity was measured on a diameter of about 20 mm.

4.2.5 Composition after post-deposition annealing

A post-deposition annealing step was necessary in order to crystallise amorphous films obtained on unheated substrates.

This study was carried out on films deposited on (0001) Al_2O_3 and (100) oxidised Si substrates using a 3" target of unreacted powder and optimal deposition conditions (Table 2).

The annealing temperature was limited to 700°C for pratical reasons (to reduce the loss of Pb, to avoid film–substrate interactions).

Figure 11 shows film composition as a function of the annealing temperature. It can be seen that the film composition was not sensitive to annealing temperature variations up to 650°C regardless of whether sapphire or silicon substrates were used.

4.3 Film structure and microstructure

The development of the film structure was examined by XRD. Figure 12 illustrates the structural development as a function of the annealing temperature (annealing time fixed to 2 h) for films deposited on (0001) Al_2O_3. The film thicknesses were about 0·75 μm. In order to suppress microcracking (due to the large difference in the coefficients of thermal expansion between film and substrate), the heating and cooling rates were optimised at 3 and 1°C/min respectively. Annealing was carried out in air.

As-deposited films produced X-ray diffraction patterns consistent with an amorphous structure.

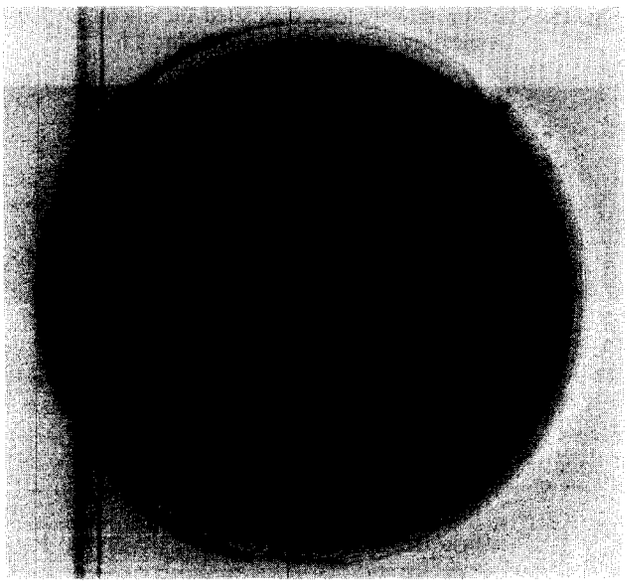

Fig. 10. Target photography after sputtering process in deposition conditions summarised in Table 3.

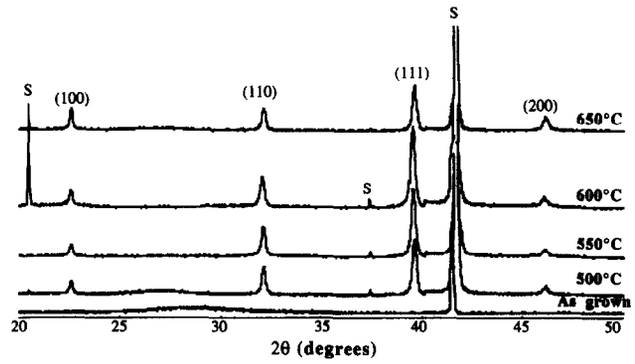

Fig. 12. XRD pattern as a function of annealing temperature for films deposited on sapphire.

The cubic perovskite structure was initiated at a temperature as low as 500°C without evidence of pyrochlore second phase. The perovskite phase formation was completed between 550 and 600°C. The same result had been reported by A. R. Kan *et al.*[13]

The PLT28 films had (111) preferred orientation on this type of substrate. At an annealing temperature of 600°C, the lattice parameter was 3·9286 Å, a value very close to that of the bulk ceramic.

It is well known that the substrate also affects crystallisation. For silicon substrates, optimal crystallisation was obtained at 650°C as can be seen in Fig. 13. These films have (110) preferred orientation. However, using the annealing parameters optimised for sapphire substrates, microcraking occurred in films deposited on silicon (Fig. 14). This was presumably due to the high stress generated at the SiO_2/PLT28 interface (large difference in the coefficients of thermal expansion). After several trials, microcracking was prevented by depositing the film with a substrate temperature of about 300°C (Fig. 15). This reduced stress in the film and perhaps initiated film crystallisation.

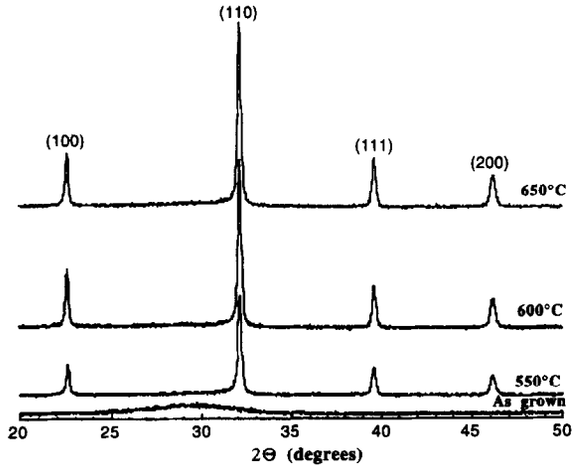

Fig. 13. XRD pattern as a function of annealing temperature for films deposited on silicon.

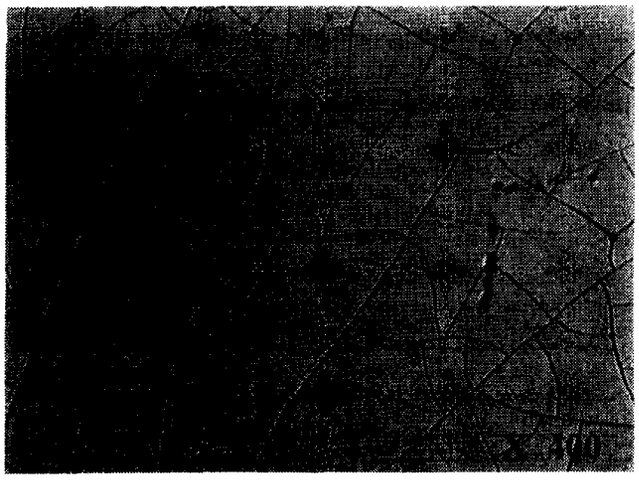

Fig. 14. Microcracking observed in the film deposited (at room temperature) on silicon after thermal treatment (600°C, 2 h).

After thermal treatment, the films were very dense as can be observed in the SEM micrograph (Fig. 16) showing the cross-section of the film annealed at 600°C for 2 h in air.

5 Conclusions

PLT28 thin films have been prepared successfully on sapphire and silicon substrates by RF magnetron sputter deposition from targets of unreacted as well as reacted powder.

The sputtering parameters have been optimised in order to assure the composition transfer between the stoichiometric target (1" and 3") and the thin film

Post-deposition annealing conditions have also been optimised to obtain crack-free PLT28 thin films with a perovskite structure on sapphire as well as on silicon substrates.

The PLT28 thin films have a (111) and (110) preferred orientation on (0001) sapphire and (100) oxidised silicon respectively.

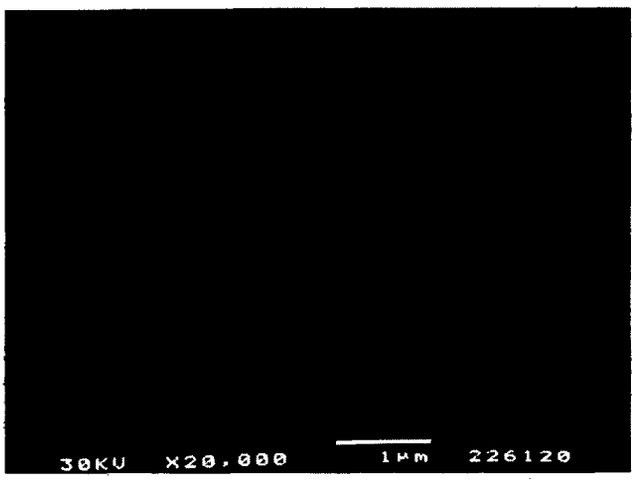

Fig. 15. The film morphology deposited on silicon at 300°C. Annealing temperature: 600°C for 2 h.

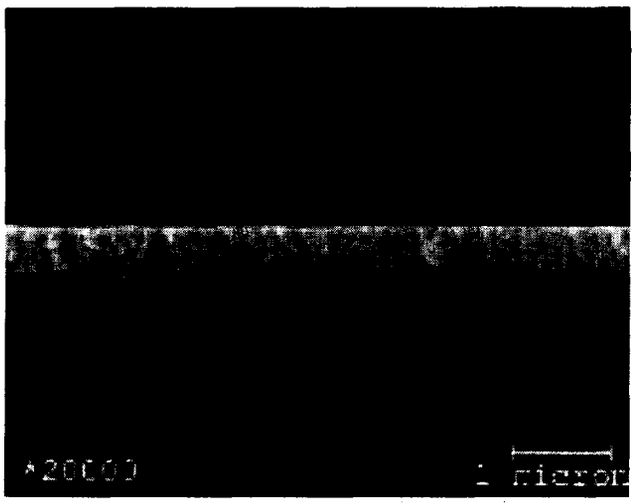

Fig. 16. Cross-section of the films deposited on silicon annealed at 650°C for 2 h in air.

References

1. Budd, K. D., Dey, S. K. & Payne, D. A., *Bl. Ceram. Proc.*, **36** (1985) 107.
2. Xu, J. J., Shaikh, A. S. & Vest, R. W. In *IEEE Transactions on Ultrasonics, Ferroelectrics and Frequency Control*, 1989 p. 307.
3. Okada, H., Takai, S., Amemiya, M. & Tominaga, K., *Jpn. J. Appl. Phys.*, **28** (1989) 1030.
4. Lijima, K., Terashima, T., Yamamoto, R., Hirata, K. & Bando, K., *Appl. Phys. Lett.*, **56** (1990) 527.
5. Ishida, M., Matsunami, M. & Tanaka, T., *J. Appl. Phys.*, **48** (1977) 951.
6. Okamura, T., Adachi, H., Shiosaki, T. & Kawabata, A., *Jpn. J. Appl. Phys.*, **30**(5) (1991) 1034.
7. Wu, A. Y., Wang, F., Bustamante, C., Yeh, C. Y. & Diels, J. C., *IEEE 7th Int. Symp. Appl. Ferro.*, Urbana-Champaign, 1990, p. 135.
8. Haertling, G. H., *Ferroelectrics*, **75** (1987) 25–55.
9. Remiens, D., Tirlet, J. F., Jaber, B., Joire, H., Thierry, B. & Moriamez, C., *J. Eur. Ceram. Soc.*,**13** (1994) 493.
10. Ishida, H., Isuji, S., Kimura, K., Matsunami, H. & Tanaka, T., *J. Crystal Growth*, **45** (1978) 393.
11. Huang, Y., Luo, W., Din, A., Ge, M. & Chen, X., *SPIE Electro-Optic and Magneto-Optic Materials and Applications*, **1126** (1989) 36.
12. Tossell, D. A., Obhi, J. S., Shorrocks, N. M., Patel, A. & Whatmore, R. W. *IEEE, Int. Symp. Appl. Ferro.*, 1992 p.11.
13. Khan, A. R., Yoo, I. K. & Desu, S. D., *Int. Symp. Appl. Ferro.*, 1992 p. 412.
14. Vassant Kumar, C. V. R. & Nansingh, A., *J. Appl. Phys.*, **65**(3) (1989) 1270.
15. Castellano, R. N., Notis, M. R. & Simmons, G. W., *Vaccum*, **27** (1977) 103.